Attenuation-Based Estimates of Rainfall Rates Aloft with Vertically Pointing K_a-Band Radars

SERGEY Y. MATROSOV

Cooperative Institute for Research in Environmental Sciences, University of Colorado, and NOAA/Environmental Technology Laboratory, Boulder, Colorado

(Manuscript received 18 March 2004, in final form 22 June 2004)

ABSTRACT

An approach is suggested to retrieve low-resolution rainfall rate profiles and layer-averaged rainfall rates, R_a, from radar reflectivity measurements made by vertically pointing K_a-band radars. This approach is based on the effects of attenuation of radar signals in rain and takes advantage of the nearly linear relation between specific attenuation and rainfall rate at K_a-band frequencies. The variability of this relation due to temperature, details of raindrop size distributions, and the nature of rain (convective versus stratiform) is rather small (~10%) and contributes little to errors in rainfall rate retrievals. The main contribution to the retrieval errors comes from the uncertainty of the difference in the nonattenuated radar reflectivities in the beginning and the end of the range resolution interval. For 2- and 1-dB uncertainties in this difference, the retrieval errors due to this main contribution are less than 34% and 17%, correspondingly, for rains with $R_a \approx 10$ mm h^{-1} at a 1-km resolution interval. The heavier rain rates are retrieved with a better accuracy since this retrieval error contribution is proportional to $1/R_a$. The retrieval accuracy can also be improved but at the expense of more coarse vertical resolutions of retrievals since the main retrieval error contribution is also proportional to the reciprocal of the resolution interval. The Mie scattering effects at K_a band results in less variability in nonattenuated reflectivities (cf. lower radar frequencies), which aids the suggested approach. Given that radar receivers are not saturated, the rainfall rates can be retrieved using cloud radars that were originally designed for measuring only nonprecipitating and weakly precipitating clouds. An important advantage of the attenuation-based retrievals of rainfall is that absolute radar calibration is not required. The inclusion of rainfall information will improve the characterization of the atmospheric column obtained with such radars used for climate research. The applications of the suggested approach are illustrated using the vertically pointing K_a-band radar measurements made during a field experiment in southern Florida. The retrieval results are in good agreement with surface estimates of rainfall rates.

1. Introduction

Ground-based millimeter-wavelength radars operating in microwave transparency ''windows'' at K_a (near 35 GHz) and W (near 94 GHz) bands were first significantly employed for atmospheric research in the mid-1980s (e.g., Pasqualucci et al. 1983; Lhermitte 1987). These radars proved to be a very valuable tool for quantitative studies of atmospheric hydrometerors from the ground and aircraft (e.g., Mead et al. 1994; Kropfli et al. 1995). The first space missions using satellite-based millimeter-wavelength radars will be launched in the near future (Stephens et al. 2002; Iguchi et al. 2002).

The initial success of research using millimeter-wavelength radars in the United States and Europe led to the development of cloud radars that have been deployed at different locations on a permanent basis for routine unattended atmospheric observations. A good and well-known example of this is the development of the K_a-band millimeter-wavelength cloud radar (MMCR) for the U.S. Department of Energy's Atmospheric Radiation Measurement (ARM) Program (Moran et al. 1998). The vertically pointing ARM MMCR radars are deployed at several Cloud and Radiation Testbed (CART) sites including the tropical western Pacific, Oklahoma, Alaska, and Australia. They have proven to be invaluable remote sensing tools at the CART sites. The ARM MMCR radars were designed and constructed by the National Oceanic and Atmospheric Administration's Environmental Technology Laboratory (NOAA/ETL). One such MMCR radar is the core part of NOAA's Portable Cloud Observatory (NPCO), which is deployed on a temporary basis at various geographical locations during different field programs.

The MMCR and different millimeter-wavelength research radars were initially designed to provide detailed, long-term observations of nonprecipitating and weakly precipitating (e.g., drizzling) clouds. A number of cloud parameter retrieval algorithms have been developed to

Corresponding author address: Dr. Sergey Matrosov, R/ET7, 325 Broadway, Boulder, CO 80305.
E-mail: Sergey.Matrosov@noaa.gov

estimate cloud microphysical properties for both ice and liquid phase clouds. These algorithms use MMCR (or similar radar) data either alone (e.g., Matrosov et al. 2002a; Mace et al. 2002) or in combination with other instrument data (e.g., Matrosov et al. 1992; Mace et al. 1998; Matrosov 1999; Frisch et al. 1995; Wang and Sassen 2001; Donovan and van Lammeren 2001; Dong and Mace 2003) to retrieve either layer-averaged cloud properties or their vertical profiles. Due to strong attenuation of millimeter-wavelength radar signals and non–Rayleigh scattering effects by raindrops, vertically pointing ground-based cloud radar measurements in rain are not usually used for quantitative rainfall retrievals, though several rain retrieval algorithms for spaceborne radars (e.g., L'Ecuyer and Stephens 2002) and scanning attenuating radars at longer wavelengths (e.g., Testud et al. 2000) have been proposed. These algorithms usually require an estimate of path-integrated attenuation.

MMCR-type cloud radars collect routine vertically resolved information on the atmospheric column, and quantitative precipitation data could be a valuable addition to this information. Vertical rainfall data can be obtained from vertically pointing radars operating at S band (around 10 GHz) or from wind profilers (e.g., Williams 2002; White et al. 2000); however, deployment of an additional radar is not always feasible for a number of practical reasons. Extension of the use of cloud radars to retrieve rainfall parameters would be useful for many scientific applications, including cloud microphysical and atmospheric radiation studies, because phase transitions significantly influence the vertical profiles of heating rates. The vertically resolved information on rain will also be valuable for model validation efforts.

Some close relations exist between the rain attenuation at K_a band and rainfall rate (e.g., Aydin and Daisley 2002; Rincon et al. 2000). In this study such relations are analyzed for different types of rain, and an attenuation-based approach is suggested for retrievals of layer-average rainfall rate above the vertically pointing K_a-band radars. The applicability of this approach is illustrated with the data in rainfall events observed by the ETL NPCO K_a-band radar during the Cirrus Regional Study of Tropical Anvils and Cirrus Layers Florida Area Cirrus Experiment (CRYSTAL–FACE) in July 2002.

2. Attenuation and backscatter of K_a-band radiation in rain for vertical incidence

The specific attenuation of the electromagnetic radiation in rain, a, and the backscatter coefficient, η, are obtained by integration over the drop equal-volume spherical diameters, D, with respect to the drop size distribution (DSD) function N (Bohren and Huffman 1983):

$$a = \left(\frac{\lambda^2}{\pi}\right) \int_0^{D_{\max}} \mathrm{Re}[S_0(D)]N(D)\, dD, \qquad (1)$$

$$\eta = \left(\frac{\lambda^2}{\pi}\right) \int_0^{D_{\max}} |S_{180}(D)|^2 N(D)\, dD, \qquad (2)$$

where λ is the radiation wavelength, the maximum drop size in rain $D_{\max}$ is about 7 mm, and $S_0(D)$ and $S_{180}(D)$ are the dimensionless complex scattering amplitudes in the forward and backward directions, respectively. Although the amplitudes $S_0(D)$ and $S_{180}(D)$ generally depend on the polarization state of the incident radiation, the polarization dependence practically vanishes for vertically pointing rain measurements, and it is ignored in further considerations.

At K_a band, the size parameters of raindrops, $x = \pi D/\lambda$, are comparable with the wavelength, and the simple Rayleigh theory is not applicable for calculations of $S_0(D)$ and $S_{180}(D)$. The Mie theory is usually used for such calculations under the assumption of sphericity of raindrops. However, raindrops with D greater than about 0.5 mm are generally nonspherical, and calculations of attenuation and backscatter generally require expansions of traditional Mie theory series to compute scattering amplitudes. In this study, the T-matrix approach (Barber and Yeh 1975) was used for computations.

For the normal atmospheric conditions, Figs. 1a and 1b show the results of calculations of the specific attenuation coefficient at the MMCR frequency as a function of the rainfall rate, R, based on DSDs measured by the Joss–Waldvogel disdrometers (JWDs) at the Kendall–Tamiami Airport during the CRYSTAL–FACE experiment in July 2002 and during the Wallops Island experiment in February–April 2001 (Matrosov et al. 2002b). The Wallops and the CRYSTAL–FACE disdrometer datasets each consisted of about 3300 1-min-average DSDs collected over a period of several months. Rainfall rates were calculated using the relation between drop sizes and their fall velocities for normal conditions at sea level (Matrosov et al. 2002b). The drop shape model used here was that from Brandes et al. (2004), who presented a drop aspect ratio–size relation compiled from several recent studies of raindrop shapes. According to this relation, raindrops are on average less oblate than predicted by the equilibrium drop shape model of Pruppacher and Pitter (1971).

Though the CRYSTAL–FACE rains were generally heavier and mostly convective in nature and the Wallops rains were colder and predominately stratiform, the a–R relations in Figs. 1a and 1b are remarkably close to each other and nearly linear. The datapoint scatter is rather small, especially for the Wallops dataset. This indicates quite low variability of a–R relations due to the details of DSD. With an accuracy better than about 10% at $R > 10$ mm h^{-1} (with the exception of a few outlying points) the following linear a–R approximation

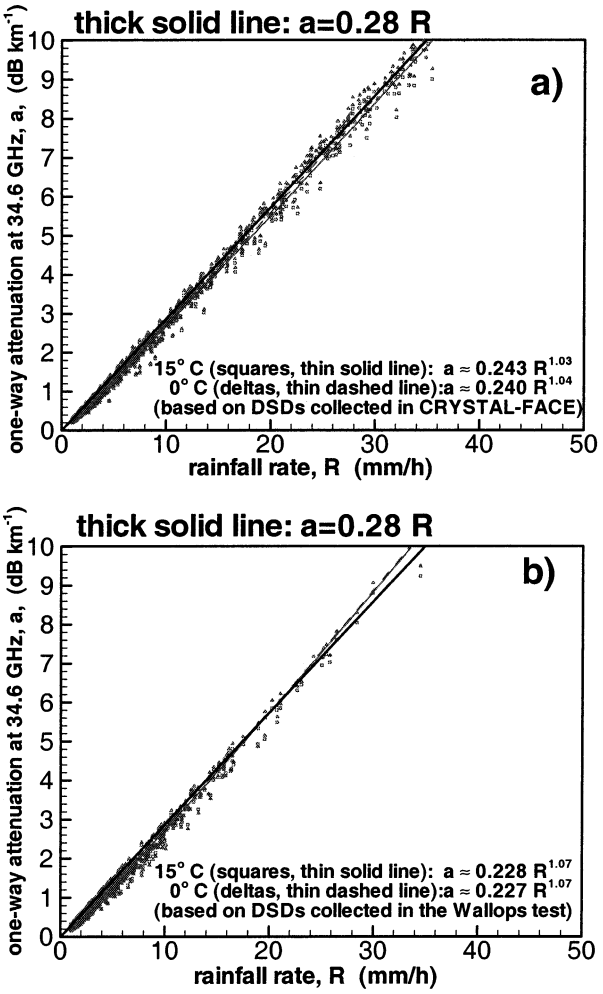

FIG. 1. Scatterplots and corresponding best-fit lines of calculated specific attenuation at 34.6 GHz vs calculated rainfall rates with the input of observed DSDs during (a) CRYSTAL–FACE and (b) Wallops field experiments.

(also shown in Figs. 1a and 1b) can be suggested for a MMCR frequency of 34.6 GHz:

$$a(\text{dB km}^{-1}) = cR(\text{mm h}^{-1}), \qquad (c = 0.28). \quad (3)$$

Figures 2a and 2b depict the scatterplots of equivalent reflectivity factor, Z_e (hereafter just ''reflectivity''), versus rainfall rate for the same DSDs. The backscatter coefficient was converted to Z_e using the conventional expression

$$Z_e = \lambda^4 \pi^{-5} |(m^2 + 2)/(m^2 - 1)|^2 \eta, \quad (4)$$

where m is the complex refractive index of water. It can be seen that the data scatter in Z_e–R relations for smaller rainfall rates is significant. However, this scatter diminishes for larger values of R. Despite this reduction in scatter for higher rainfall rates, reflectivity-based estimators in K_a band are not a viable option for rainfall retrievals due to strong attenuation.

There is obvious general flattening of Z_e–R relations for $R > 5$ mm h^{-1}, which is mostly due to non-Rayleigh effects. As will be shown later, this effect is advantageous for the attenuation-based estimation of rainfall. Overall, the relations shown in Figs. 2a and 2b (e.g., $Z_e = 407R^{1.29}$ for CRYSTAL–FACE and $Z_e = 324R^{1.44}$ for Wallops at 15°C) are in general agreement with a relation at K_a band used by Meneghini et al. (1989): ($Z_e = 355R^{1.26}$).

For a purpose of illustration, Figs. 2c and 2d show the a–Z_e scatterplots calculated for the two considered DSD sets. The data scatter in the a–Z_e relations is much larger than that for a–R relations and is quite similar to the one for Z_e–R relations. The stability of the a–Z_e relations, and especially the constancy of the exponent in the best-fit $a = f(Z_e)$ power law approximation is essential when applying the Hitschfeld and Bordan (1954) approach, which is sometimes used for retrieving the rainfall rate at attenuating radar wavelengths (e.g., Testud et al. 2000). It can be seen from the best-fit approximations in Figs. 2c and 2d that this exponent at K_a band changes quite significantly: from around 0.81 for the CRYSTAL–FACE data to about 0.73 for the Wallops data. Another reason that hampers the use of the Hitschfeld and Bordan approach for vertical rain profiling with ground-based K_a-band radars is the requirement for integrating attenuated radar reflectivities for the whole rain layer. As will be shown later, K_a-band cloud radar measurements in rain are often saturated near the ground and no attenuated reflectivity data are available when radar receivers are in the saturation regime. Here, the suggested approach to retrieve rainfall rate directly from the K_a-band attenuation estimates makes use of the linear stability of the a–R relations.

a. Temperature and drop shape dependence of a–R and Z_e–R relations

To evaluate the drop shape dependence of a–R and Z_e–R relations, calculations were also performed for equilibrium drop shape. These calculations revealed very small changes compared to the results shown in Figs. 1 and 2, thus indicating a weak dependence of radar parameters on drop shape at vertical incidence. The changes due to the drop shape model were typically within a few percent, and the a–R and Z_e–R relations for equilibrium shape are not presented here.

Figures 1a and 1b show the a–R relations calculated for two temperatures: 0° and 15°C. It can be seen that corresponding changes are very small and within the previously stated uncertainty due to DSD details. This negligible temperature dependence in attenuation at K_a band is in stark contrast to noticeable attenuation variability due to temperature changes at longer radar wavelengths. The temperature variations between 15° and 0°C at X band, for example, can result in about 10% changes in specific attenuation (Matrosov et al. 2002b). The difference in the attenuation temperature dependence at different radar frequencies can be ex-

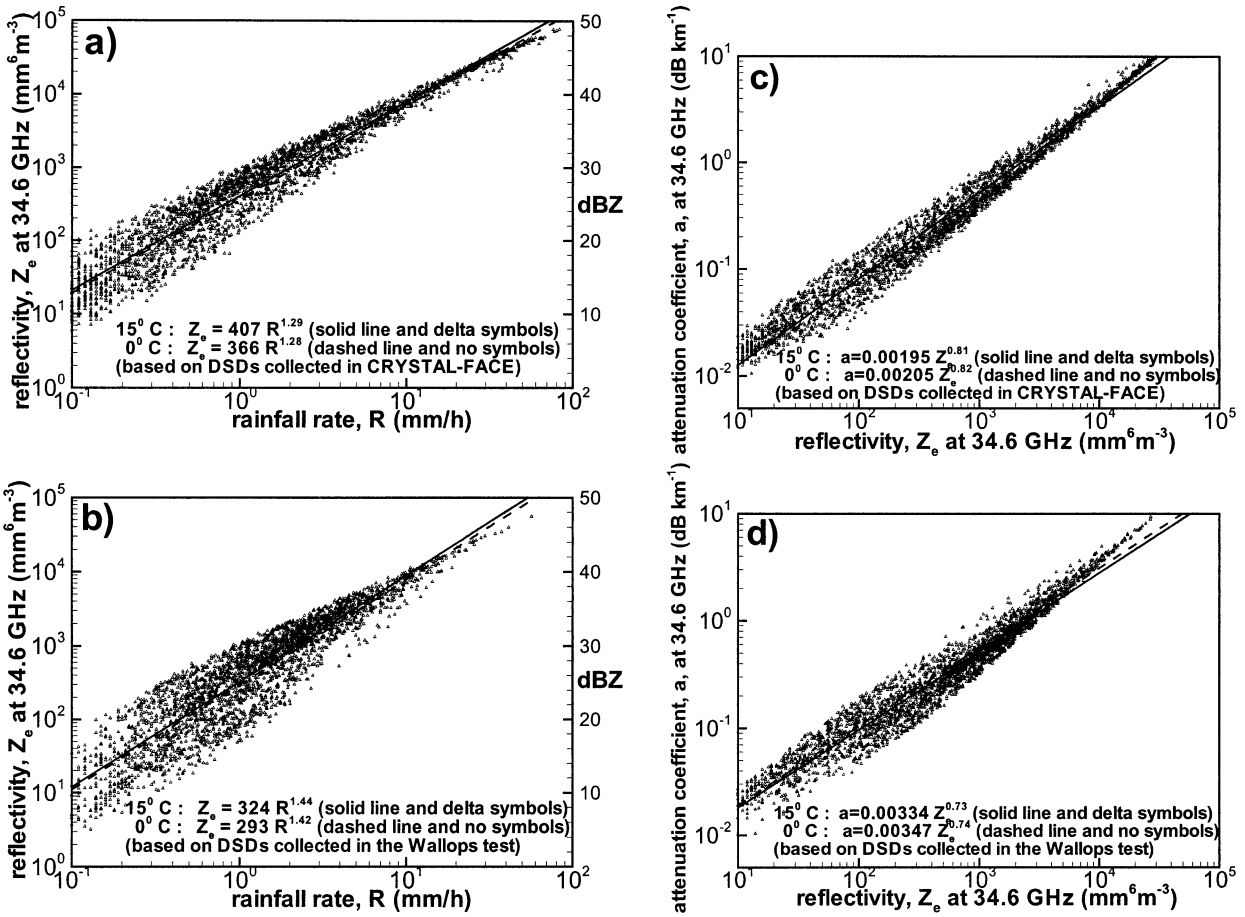

FIG. 2. As in Fig. 1 but for the (a), (b) radar reflectivity vs rainfall rate and (c), (d) extinction coefficient vs radar reflectivity.

plained by analyzing the extinction (i.e., attenuation) efficiency expansion with respect to size parameter, x (Bohren and Huffman 1983):

$$Q_{\text{ext}} = 4x\text{Im}\{(m^2 - 1)(m^2 + 2)^{-1} \times [1 + 0.067x^2(m^2 - 1)(m^2 + 2)^{-1} \times (m^4 + 27m^2 + 38)(2m^2 + 3)^{-1}]\} + 2.67x^4\text{Re}[(m^2 - 1)^2(m^2 + 2)^{-2}]. \quad (5)$$

The first term in (5) is responsible for the Rayleigh-type effects and is dominant at larger λ. It decreases noticeably as temperature increases. The second and the third terms in (5) increase with temperature, and the contributions from these terms also increase as non-Rayleigh effects become more pronounced at higher radar frequencies. At K_a band, as temperature increases, a decrease in the first term is approximately offset by an increase in the second and third terms, resulting in a very weak temperature dependence. Though (5) is strictly applicable only for spherical particles, this explanation is still valid for slightly nonspherical drops because the effects of nonsphericity at vertical incidence are rather small.

The temperature variability of Z_e–R relations is generally more significant than that of a–R relations. A temperature increase from 0° to 15°C generally results in an increase in backscatter coefficients. For comparison, best-fit power law Z_e–R relations are shown in Figs. 2a and 2b for 0° and 15°C.

The data presented show that the attenuation–rainfall rate relations at K_a band are quite remarkable in the sense that they are nearly linear and do not exhibit significant variabilities due to details of DSD or temperature changes. These properties make these relations a convenient tool for attenuation-based approaches for estimating rainfall rates.

b. *Possible effects of drop undercount in JWD raindrop spectra*

Impact disdrometers such as JWD are known for some undercount of smaller (<1 mm) and very large drops (Tokay and Short 1996). However, the a–R relations that are used for the retrievals here are practically linear and show very little variation with respect to DSD details. This means that both the extinction coefficient and the

rainfall rate are proportional to approximately the same moment of DSD. Adding drop counts in the small (or large) JWD size bins causes a particular datapoint move along the linear *a–R* relation but practically does not change this relation. In other words, missing drops add approximately the same relative amount in both *R* and *a.* Numerical experiments with experimental JWD DSD spectra were performed. During these experiments drop counts in the smaller and large drop bins were added to the experimental JWD DSD spectra, so the *a* and *R* individually would change as much as 10%. The corresponding relative deviations from the original *a–R* relation did not exceed a few percent. This indicates the stability of the derived *a–R* relations at K_a band to potential drop undercounts.

3. Retrievals of rainfall rate based on K_a-band attenuation estimates

Assuming a uniform layer of rain, an estimate of rainfall rate is proportional to the vertical range (h) derivative of the reflectivity expressed in logarithmic units:

$$R(\text{mm h}^{-1}) = k(2c)^{-1}(\partial Z_{\text{el}}/\partial h), \tag{6}$$

where $Z_{\text{el}}(\text{dB}Z) = 10 \log_{10}[Z_{\text{el}}(\text{mm}^6\ \text{m}^{-3})]$, h is the height above the radar (in km) and the coefficient $c = 0.28$ dB km^{-1} h mm^{-1} is from (3). The dimensionless coefficient k accounts for the raindrop fall velocity changes due to changing air density, ρ, aloft (Matrosov et al. 2002a):

$$k(h) \approx 1.1\rho(h)^{-0.45}, \tag{7}$$

where the air density is in kilograms per cubic meter.

In reality, the vertical profile of nonattenuated reflectivity in rain is generally not constant. An average value of rainfall rate, R_a in a vertical layer with a geometrical thickness of Δh, can be estimated as

$$R_a(\text{mm h}^{-1}) = k(2c)^{-1}(\Delta Z_{\text{el}}/\Delta h), \tag{8}$$

where ΔZ_{el} is the difference of reflectivities at the base and the top of the layer considered and the coefficient k is applied to the middle of this layer.

Equation (8) assumes that the two-way attenuation effect of the rain layer is dominant compared to the changes in the actual reflectivity within the layer. This attenuation effect linearly increases with the rainfall rate and with the layer thickness. It can be seen from Figs. 1a and 1b that for $R > 15$ mm h^{-1} and $\Delta h = 0.5$ km, the two-way attenuation is already about 4.2 dB. Since attenuation increases with rainfall rate, it is expected that estimates from (8) will be more accurate for higher rainfall rates. This is aided by the fact that, due to non-Rayleigh backscatter at K_a band, actual (nonattenuated) reflectivities on average increase with rainfall rate at a lower rate (compared to longer radar wavelengths) for higher values of *R.* Figure 3 illustrates this fact by showing details of the correspondences between Z_e and R at the higher rainfall rates.

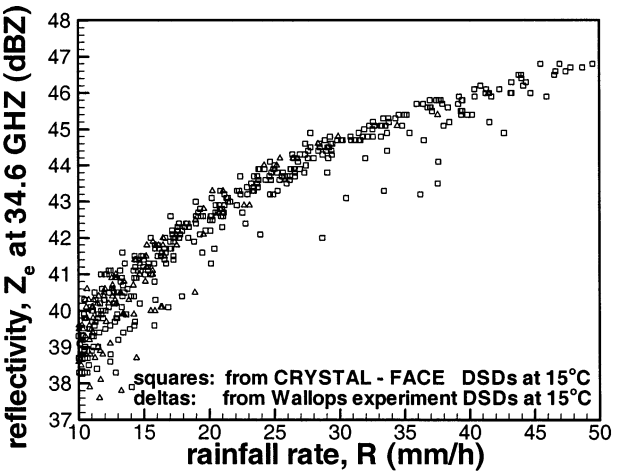

FIG. 3. The K_a-band radar reflectivities for higher rainfall rates showing effects of non-Rayleigh scattering.

It can be seen from Fig. 3 that data from both Wallops and CRYSTAL–FACE DSDs occupy the same scatter area. For $R > 15$ mm h^{-1}, the highest possible dynamic range of nonattenuated reflectivities is less than about 6–7 dB. For $R > 25$ mm h^{-1}, this dynamic range is typically less than 4 dB. Given this fact, for higher rainfall rates, the dominance of the decrease in reflectivity due to attenuation over the variability of nonattenuated reflectivity can easily be achieved for already modest layer thicknesses Δh. Furthermore, since a variability in a vertical profile of nonattenuated reflectivity is not expected typically to be higher than 2 dB km^{-1} (Smyth and Illingworth 1997), the attenuation effects will dominate the possible variability in nonattenuated Z_e in the observed values of ΔZ_e at intervals $\Delta h = 0.5$ km beginning from the rainfall rates of about 7 mm h^{-1}.

The approach described above to estimate layer-average rainfall rate assumes that the nonattenuated reflectivities are not known and simply relies on the dominance of the attenuation effects. In some cases, a reference reflectivity can be available from the high clouds that are located above the rain layer. If this reference reflectivity, $Z_{\text{el}}^{(r)}$, does not change significantly over the period of the rain event (e.g., during quick passing convective rain shafts), the logarithmic reflectivity difference due to attenuation in (8) for the whole rain layer can be estimated as

$$(\Delta Z_{\text{el}}) = Z_{\text{el}}^{(r)} - Z_{\text{el}}^{(a)}, \tag{9}$$

where $Z_{\text{el}}^{(a)}$ is the observed (i.e., attenuated) reflectivity of a reference cloud measured in the presence of a rain shaft, and $Z_{\text{el}}^{(r)}$ is the reference reflectivity in the absence of rain. This is similar in concept to the spaceborne radar technique of using the ocean surface backscatter as a reference for downlooking rain retrievals (Meneghini and Kozu 1990).

The CRYSTAL–FACE experiment provided observational events that were used to illustrate both versions

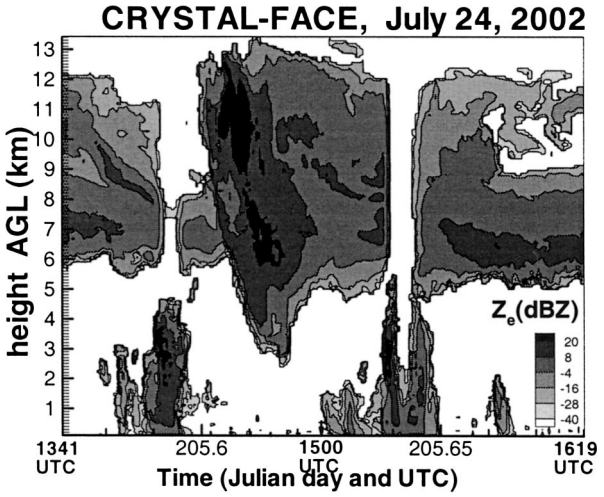

FIG. 4. Time–height cross section of the reflectivity values measured by the ETL vertically pointing K_a-band radar during the 24 Jul 2002 observation case in CRYSTAL–FACE.

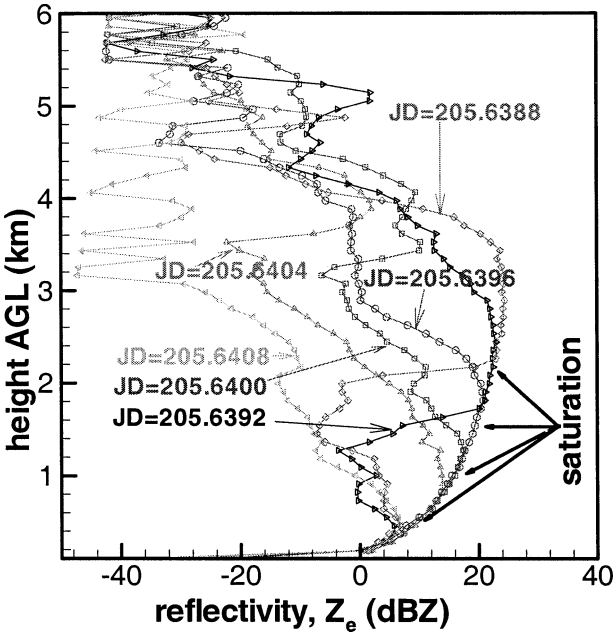

FIG. 5. Several consecutive vertical profiles of the reflectivities measured by the ETL K_a-band radar in the precipitation mode during the heavy convective rain event.

of the approach (i.e., with and without the reference reflectivity) for attenuation-based retrievals of rainfall rates from vertically pointing K_a-band cloud radar measurements. The ETL MMCR radar was deployed along with other ground-based instruments at the eastern ground validation site at the Kendall–Tamiami Airport. The NOAA Aeronomy Laboratory's Joss–Waldvogel disdrometer was practically collocated with the radar, and its data were used for comparisons with radar retrievals.

a. Estimations of rainfall rates based on reflectivity gradients

Figure 4 shows a cross section of the radar reflectivity measured by the ETL MMCR radar over about 2.5 hours on 24 July 2002. A very thick cloud extended from about 5 km to almost 13 km above ground level (AGL). Several convective rain shafts moved over the radar site during this period. The shower centered at about 1530 UTC [Julian day (JD) 205.646] was the heaviest. In the middle of the duration of this shower, the radar signals were completely attenuated beyond about 2.5 km AGL for a period of about 4 min. Cloud echoes above 5 km AGL were not seen for about 8 min due to complete extinction.

Several vertical profiles of measured reflectivity Z_{el} during this strong shower are shown in Fig. 5. During the CRYSTAL–FACE data collection period, ETL MMCR cycled over four different measurement modes, with each mode taking about 9 s of measurement time. Different modes were designed to better cover various hydrometeor species in a range from the ground to about 17 km AGL. The so-called precipitation mode had the largest unambiguous ''folding'' vertical Doppler velocity range (± 15.1 m s^{-1}) and saturated at stronger echoes compared to other modes designed to measure weaker cloud echoes. Data shown in Fig. 5 represent consecutive profiles taken in the ''precipitation mode.'' The saturation level of this mode is clearly seen in the Fig. 5 data, and it is about 16 dBZ at 1 km (22 dBZ at 2 km). The noise level of this mode is about -25 dBZ at 5 km. The data in the nearest vicinity beyond the saturation (three to four resolution cells) are in a regime that is transitional from the receiver saturation to the linear receiver regime. The data points beyond this transitional regime are believed to be in the linear range and are suited for rainfall estimations using the approach discussed above.

The reflectivity decrease in the linear receiver regime for displayed profiles is quite monotonic except for a few spikes. This decrease is quite rapid as height AGL increases, which suggests the dominance of the attenuation effects. Equation (8) was used to estimate an average rainfall rate R_a in a 500-m-thick layer centered at about 2.5 km AGL for profiles after JD 205.6395 (1521 UTC). The estimates for lower heights AGL were not possible due to the saturation of radar echoes at closer ranges (see Fig. 5). The corresponding attenuation-based rainfall retrievals are shown in Fig. 6. The retrieval points in Fig. 6 prior to JD 205.6395 correspond to the layer centered at about 3.1 km AGL since at this time radar signals were in saturation at lower ranges. Radar estimations show a profound rapid increase in rainfall rate to a peak of about 48 mm h^{-1} followed by a quick decrease.

The DSD data from a collocated disdrometer were used to calculated ground-level rainfall rates at the radar site. The corresponding estimates are also shown in Fig.

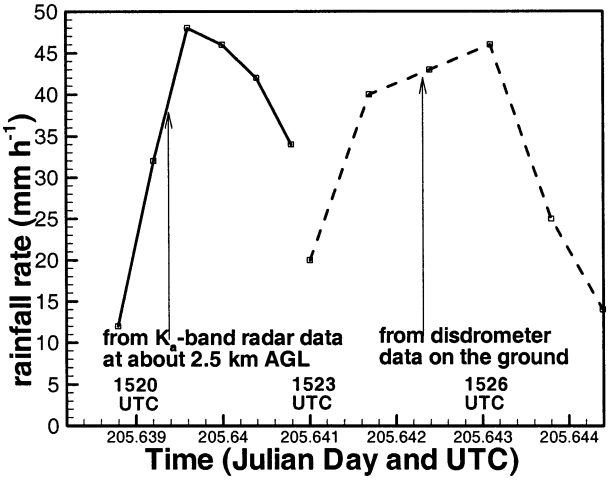

FIG. 6. Comparisons of rainfall rates retrieved from the radar data and estimated from the disdrometer measurements at the ground near the radar site.

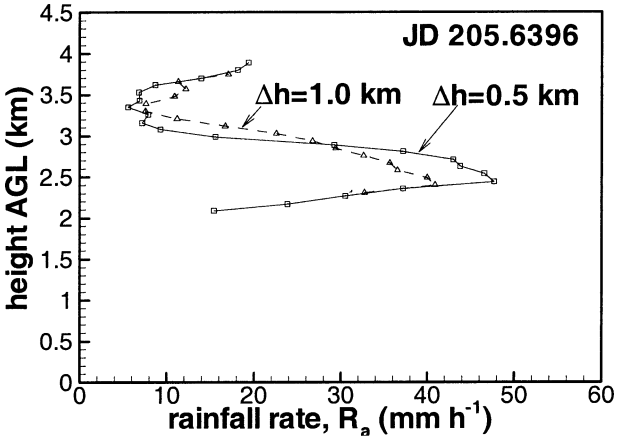

FIG. 7. Retrievals of vertical profiles of rainfall rate at JD 205.6396 with two different resolutions Δh.

6. It can be seen that disdrometer-derived rainfall rates also show a similar shape in rainfall rate with a peak at about the same value as the radar retrievals, though the ground rainfall peak is observed about 5 min later. This time difference can be explained by the time required for this heavy rainfall cell to reach the ground from an altitude of about 2.5 km AGL. Typical Doppler velocities measured by the radar at this altitude (not shown) were about 8 m s^{-1}. Horizontal advection effects and vertical changes in rainfall were probably occurring, so one cannot expect a perfect match between the rain aloft and the later rain on the ground. Nevertheless, the qualitative and, to some extent, quantitative agreement between radar-derived rainfall rates and those calculated from disdrometer-derived DSDs provides a certain confidence in radar retrievals.

Figure 7 shows retrievals of the rainfall-rate vertical profiles at JD 205.6396 with two different resolutions: $\Delta h = 0.5$ km and $\Delta h = 1$ km. The sliding window with corresponding Δh intervals were used for the retrievals, so the data are shown at each range gate. The retrievals were not available below 2 km due to saturation and above about 4 km due to complete extinction of the radar echoes. A layer of heavy rain between 2 and 3 km AGL, which later reached the ground, is evident. There is a general agreement between retrievals with different resolutions. The retrieval uncertainty decreases as Δh increases, though larger Δh results in smoothing of the results. The retrieval uncertainties are discussed in detail in section 4.

b. Estimations of layer-mean rainfall rates in the presence of reference reflectivity

As can be seen from Fig. 4, another convective rain shaft quickly moved over the radar site at around JD 205.59 (1410 UTC). The duration of the rain event associated with it was comparable to the shaft discussed in the previous subsection; however, this rain was not as strong as the one around 1530 UTC, so the cloud echoes above the rain layer were not completely attenuated, though they were very significantly reduced. A thin sliver of weak cloud echo is present at 7.6 km AGL. The rain shaft extended to about 4.5 km AGL. The radiosonde soundings and numerical forecast model runs at around the time of the event indicated a freezing level at about 5 km AGL, so all precipitation echo around 1410 UTC was warm rain.

Figure 8 shows the cloud reflectivity at 7.6 km AGL for the entire period shown in Fig. 4 as a time–height cross section. The periods of complete and partial attenuation due to rain are clearly identified. For the rest of the time period in Figs. 8 and 4, cloud reflectivity at 7.6 km AGL was around 5 dBZ $\pm$ 3 dBZ except for a short period at around JD 205.61 (1439 UTC), when a

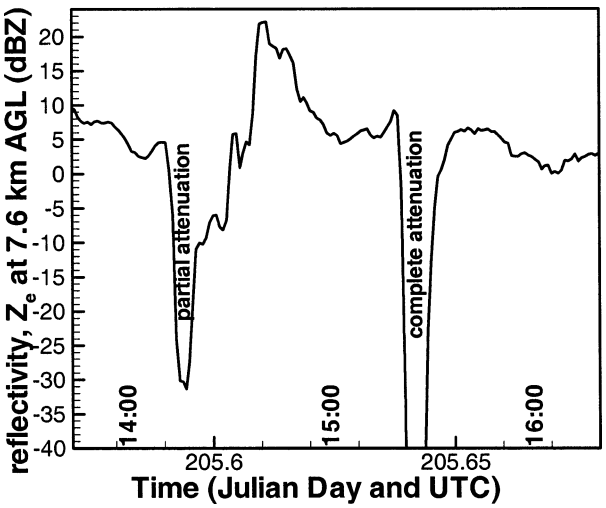

FIG. 8. Radar reflectivity at 7.6 km AGL for the observational event shown in Fig. 4.

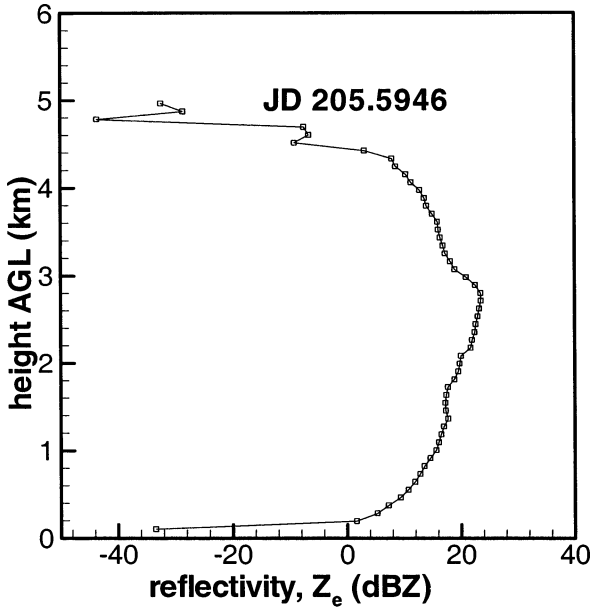

FIG. 9. The reflectivity profile measured by the ETL K_a-band radar in the precipitation mode at JD 205.5946.

heavier cloud fall streak reached an altitude of about 3 km AGL, as seen in Fig. 4.

The leading edge of the moderate rain shaft passed above the radar site at JD 205.59. Measured reflectivities in the 0–1.5 km AGL layer just prior to JD 205.59 were smaller than -10 dBZ and did not exhibit much of vertical variability. This generally corresponds to rainfall rates less than about 0.1 mm h^{-1}, and the corresponding attenuation can be neglected. As seen from Fig. 8, the movement of this leading edge resulted in a sharp decline of cloud reflectivity at 7.6 km AGL by about 30 dB. Substituting $\Delta Z_{el} = 30$ dB in (8), one can obtain a layer-average rainfall rate of about $R_a \approx 11$ mm h^{-1} for this moderate rain shaft with geometrical layer thickness $\Delta h \approx 4.5$ km. The estimate from the ground disdrometer-derived DSD at JD 205.595 is about 8 mm h^{-1}, which is somewhat smaller than the radar estimate. However, given probable vertical nonhomogeneity of rain and the horizontal advection effects, the agreement between radar and disdromer-based estimates can, probably, be considered satisfactory.

Some of the rain vertical nonhomogeneity is evident from Fig. 9, which depicts the vertical profile of measured radar reflectivity for the time corresponding to the middle of the discussed rain shaft at JD 205.5946. The radar signals below 3 km are effectively saturated or they are in the regime that is transitional from the saturation and linear receiver regimes. Rainfall estimates, however, can be made for heights above 3 km using the gradient approach. Using (8) for the reflectivity data in the profile shown in Fig. 9 results in $R_a \approx 9$ mm h^{-1} for the 500-m layer between 3 and 3.5 km, and $R_a \approx 13$ mm h^{-1} for the 500-m layer between 3.5 and 4 km.

4. Assessment of attenuation-based rain retrieval errors

a. Assessment of retrieval errors for presented experimental examples

By their nature, attenuation-based rainfall rate retrievals at K_a band cannot produce high-resolution estimates. However, an about 0.5–1-km vertical resolution or the entire rain layer-averaged rainfall rates have their own value, and the accuracy of their retrievals can be better than that for traditional radar methods based on reflectivity measurements at longer wavelengths. When higher cloud reference reflectivity is present, as discussed in section 3b, the relative retrieval error $(\delta R_a/R_a)$ for the average value of rainfall rate R_a in the entire rain column is determined, in large part, by the accuracy of estimating the nonattenuated reference reflectivity, $Z_{el}^{(r)}$. It can be seen from Fig. 8 that $Z_{el}^{(r)}$ values immediately before and after the rain event at around JD 205.59 were at about the same level with an uncertainty of about 3 dB. This translates into about a 10% uncertainty in the ΔZ_{el} estimate (i.e., $\Delta Z_{el} = 30$ dB $\pm$ 3 dB), which, coupled with about 10% uncertainty of the specific attenuation–rainfall rate relations [i.e., an uncertainty in the coefficient c in (3)], yields an estimate of $\delta R_a/R_a \approx 0.15$ assuming independence of the error contributions:

$$(\delta R_a/R_a)^2_{\text{total}} = (\delta R_a/R_a)^2_c + (\delta R_a/R_a)^2_z, \qquad (10)$$

where the terms in the right-hand side of (10) represent the error contributions from uncertainties in the coefficient c and in the ΔZ_{el} estimate.

It is important to mention that the attenuation-based rainfall retrievals do not depend on the uncertainty of the absolute radar calibration because they use relative and not absolute reflectivity measurements. Partial attenuation caused by a wet antenna or radome does not affect the rainfall estimates either. In the example in which reference cloud reflectivity is used, there is probably no significant contribution from the gaseous attenuation uncertainty at K_a band (Matrosov et al. 2004), assuming that this contribution is about the same for rain-free and rain-filled profiles.

For heavier rain events when, due to complete attenuation of radar signals, there is no reference cloud reflectivity, layer-averaged rainfall rate retrievals have higher uncertainties. These uncertainties, however, generally diminish as rainfall rate increases since the variability of nonattenuated reflectivities becomes smaller due to non-Rayleigh scattering effects and the attenuation effects become progressively more dominant. The accuracy of rainfall retrievals will improve as the difference between the actual (i.e., nonattenuated) reflectivities in the beginning and the end of the layer for which R_a is estimated become smaller, compared to reflectivity changes due to attenuation.

For stratiform rain events, actual radar reflectifity values below the bright band usually do not vary significantly (Smyth and Illingworth 1997). The experience

with X-band measurements in such rains indicated typical changes of only a few decibels over the entire rain layer (Matrosov et al. 2002b). For convective (nonbrightband events), Smyth and Illingworth (1997) report an about 2 dB km^{-1} S-band reflectivity increase with diminishing altitude AGL. Nonattenuated reflectivity changes at K_a band should be even smaller than those at X and S bands. Though vertical profiles of nonattenuated reflectivity typically are not expected to vary significantly, the situations can occur when streamers of heavier precipitation are tilted by wind shear. These can form elevated gradients of nonattenuated reflectivity with height and complicate the retrievals. Such situations are usually recognizable by observing the radar echo patterns.

Given the above nonattenuated reflectivity variability estimates, it was assumed when assessing the accuracy of radar retrievals of R_a shown in Fig. 6 that the actual reflectivities at the start and the end of 500-m layers used to estimate R_a can differ on average by about 2 dB. This 2-dB variability value amounts to only 14% of the total reflectivity change over the considered 500-m interval at the maximum of estimated $R_a \approx 48$ mm h^{-1} (JD 205.6396) and 27% for JD 205.6392 when the layer-averaged rainfall rate was estimated as $R_a \approx 26$ mm h^{-1}. Using (10) and assuming the 10% uncertainty in the coefficient c, the total retrieval errors can be estimated as about 17% for $R_a \approx 48$ mm h^{-1} and about 29% for $R_a \approx 26$ mm h^{-1}. Note that increasing the layer thickness can decrease the layer-averaged retrieval uncertainty because it increases the attenuation contribution to the total drop of measured reflectivity over the considered layer interval.

b. General assessment of retrieval errors

Using (8), it can be shown that the terms in (10) can be given as

$$(\delta R_a/R_a)_c = \delta c/c, \tag{11}$$

$$(\delta R_a/R_a)_z = 0.5\delta Z_{\rm el} k(c\Delta h R_a)^{-1}, \tag{12}$$

where $\delta Z_{\rm el}$ is the difference between nonattenuated reflectivities in the beginning and the end of the interval Δh for which the estimate R_a is derived.

Figure 10 shows the relative retrieval errors for different values of $\delta Z_{\rm el}$ and Δh as a function of R_a. As before, $\delta c/c$ was assumed to be 0.1. It can be seen that for given values of $\delta Z_{\rm el}$ and Δh the retrieval error for smaller values of R_a is determined mostly by the uncertainties in the nonattenuated reflectivity difference, and it diminishes as R_a increases as the attenuation effects are becoming progressively more dominate over this difference. As R_a increases, the role of the uncertainty of the coefficient c in the linear a–R relation is becoming increasingly more important and is becoming a dominant factor in the retrieval error for larger Δh and R_a values.

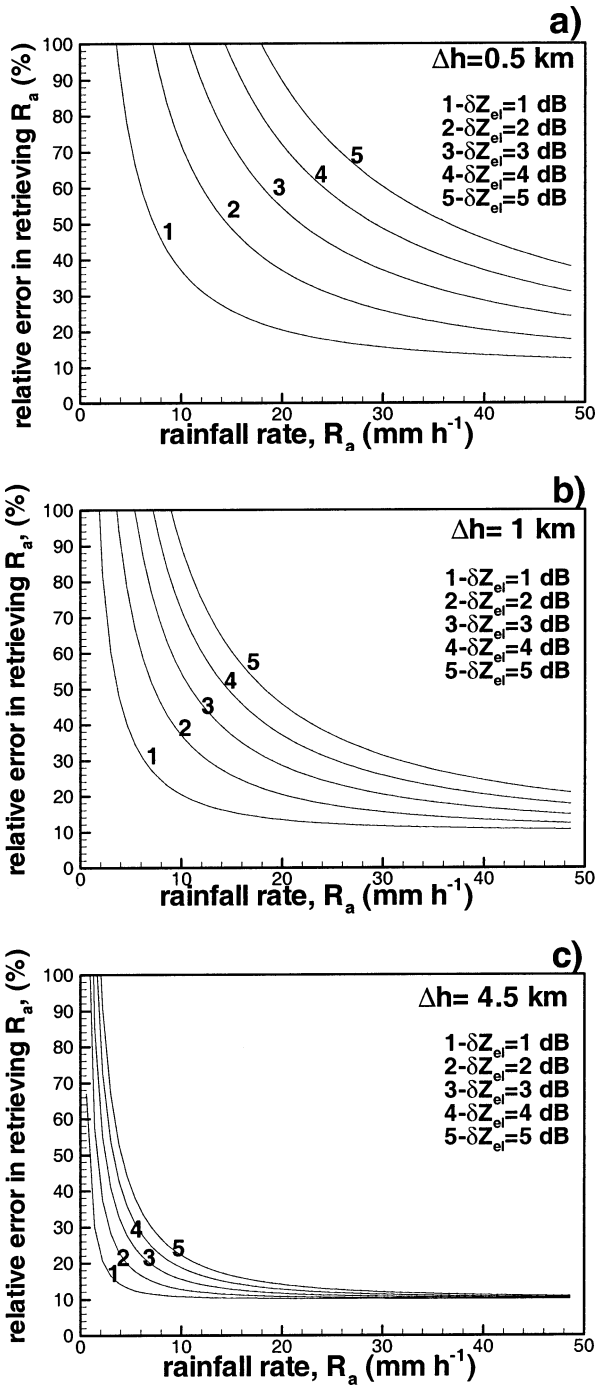

FIG. 10. Relative errors of rainfall rate estimates for different vertical resolutions Δh, and uncertainties in the differences of nonattenuated reflectivities in the beginning and the end of the estimation interval $\delta Z_{\rm el}$.

For $\Delta h = 1$ km (Fig. 10b), the relative retrieval error of R_a is better than 30% for $R_a > 6$ mm h^{-1} if $\delta Z_{\rm el} = 1$ dB and for $R_a > 12$ mm h^{-1} if $\delta Z_{\rm el} = 2$ dB. For $\Delta h = 0.5$ km (Fig. 10a) and smaller rainfall rates, the retrieval errors are roughly twice as high as for

$\Delta h = 1$ km for the same values of δZ_{el}, though one would expect less variability of nonattenuated reflectivities at smaller distances Δh. For higher rainfall rates, the retrieval errors could be pretty reasonable, even for the 0.5-km resolution, especially in stratiform rains when δZ_{el} is expected to be small.

At the 1-km resolution (Fig. 10b), the retrieval errors are less than about 50% for all rain rates greater than approximately 17 mm h^{-1}, even for the uncertainty in the nonattenuated reflectivity difference $\delta Z_{el} = 5$ dB. It should be mentioned that for such rainfall rates, 5–6 dB is as much as this difference can possibly be due to non-Rayleigh scattering (see Fig. 3). In other words, for $R_a > 17$ mm h^{-1} and $\Delta h = 1$ km, the maximum possible retrieval error is close to 50%. In reality the actual error will be smaller since the worst case scenario was considered in this example. Increasing Δh will further reduce the expected error (at the expense of resolution, though) since the main error contribution is proportional to $1/\Delta h$, as can be seen from (12).

Figure 10c corresponds to $\Delta h = 4.5$ km and can be used to estimate retrieval errors for all of the rain layer-mean values, as described in section 3b. In this case δZ_{el} is the uncertainty in the reference reflectivity. It can be seen that even a rather high value of $\delta Z_{el} = 5$ dB results in rather reasonable retrieval errors for $R_a > 6$ mm h^{-1}. For larger rainfall rates $R_a > 20$ mm h^{-1}, the main contribution to the retrieval error comes from the uncertainty in the coefficient c in (3) and (11).

5. Conclusions

It has been demonstrated that vertically pointing K_a-band cloud radars can be successfully used for retrievals of low-vertical-resolution rainfall rate profiles and average rainfall rates in the rain layers. These retrievals are based on attenuation effects and utilize the general linearity of the rainfall rate (R)–specific attenuation coefficient (a) relations at K_a-band radar frequencies. The retrieval approaches are aided by the negligible temperature dependence of these relations and their low susceptibility to the details of the raindrop size distributions. The combined variability of a–R relations due to DSD details and temperature does not generally exceed about 10% for $R > 5$ mm h^{-1} for both stratiform (i.e., below brightband) and convective (i.e., nonbrightband) rains.

In cases when the higher cloud reference reflectivity is known with an acceptable degree of certainty just prior and after the rain event and can be measured for the periods when the rain is present, an average rainfall rate for the entire rain layer, R_a, can be estimated in a rather straightforward way. A retrieval error of such estimates is mostly determined by the ratio of the uncertainty of the nonattenuated reference reflectivity during the rain event and the magnitude of the higher cloud reflectivity dip due to rain attenuation. Using ground-based K_a-band data from CRYSTAL–FACE, it was demonstrated that this approach can be successfully applied for convective shafts of warm rain quickly passing over the radar deployment site. An estimated retrieval error can be as low as about 15%–20% for moderate rainfall rates of around 10–15 mm h^{-1}. The reference approach is best when applied to short duration showers because the reference cloud is more likely to maintain a reasonably steady reference reflectivity.

Using the gradient approach, rainfall rates R_a greater than about 5–10 mm h^{-1} can also be successfully retrieved with a spatial layer resolution of about 0.5–1 km in rain areas where radar echoes are neither in saturation nor in complete extinction. Vertical gradients of radar reflectivity due to attenuation in such layers should be greater than typical changes due to a natural variability of nonattenuated reflectivities. This requirement is alleviated by non-Rayleigh scattering effects, which cause the nonattenuated reflectivities to vary less with rainfall rate at K_a band compared to longer radar wavelengths that are typically used for radar rainfall studies. The errors of rainfall rate retrievals based on gradients are determined by the uncertainty in the linear a–R relation coefficient and by the uncertainty in the differences (δZ_{el}) between nonattenuated reflectivities, in the beginning and the end of the layer resolution interval Δh used for retrievals. The latter error source is usually dominant for Δh values that are less than about 1 km and is proportional to $1/\Delta h$. The relative retrieval errors decrease as R_a increases. For $\delta Z_{el} = 2$ dB and $\Delta h = 1$ km the relative retrieval errors are about 35% for $R_a \approx 10$ mm h^{-1} and 20% for $R_a \approx 20$ mm h^{-1}.

Retrievals of rainfall rates using the suggested gradient approach were demonstrated using the CRYSTAL–FACE data obtained in a heavy downpour during which radar signals were completely attenuated above about 3 km AGL. In the region where the radar receiver was not saturated, retrieval estimates of rainfall rates during this event were larger than 10 mm h^{-1} with the maximum 500-m layer-averaged values exceeding 45 mm h^{-1} at about 2.5 km AGL. Saturation of the radar signals at lower ranges AGL prevented retrievals near the ground. The radar-retrieved values were in good agreement with ground-based estimates from DSD recorded by the Joss–Waldvogel disdrometer a few minutes later when the rain observed by the radar aloft reached the ground. The retrieval uncertainties of radar estimates for these layer-mean values were estimated as 17%–28% for $R_a \geq 25$ mm h^{-1}.

Though not a substitute for the methods used with vertically pointing longer-wavelength radars, the demonstrated approaches for rainfall retrievals can be used with vertically pointing K_a-band cloud radars that, like DOE ARM MMCR radars, routinely collect information in the atmospheric column at different test-bed sites. This would allow a more complete characterization of the atmospheric column above these sites by including rainfall periods. This is especially important for validating phase-transition processes in atmospheric column

models. Though the proposed method suggests retrievals of rainfall rates aloft, it can be potentially generalized for estimating vertical structure of rain liquid water contents using relations between these contents and *R*. This generalization, however, is outside the scope of the current study.

Attenuation-based retrievals are limited to the altitudes where radar echoes are neither in saturation nor in complete extinction. The usable altitude range depends on the dynamic range, receiver gain, radar sensitivity, and some other radar parameters as well as on the rain intensity. Parameters of the precipitation measurement mode of cloud radars can be adjusted to better accommodate needs for attenuation-based rain rate retrievals and tuned to rain climatologies characteristic to particular sites.

One important advantage of the attenuation-based retrievals is that they do not require an absolute calibration of the radar. Inevitable uncertainties in the radar absolute calibration could reach a few decibels and can contribute significantly to errors in the retrievals that use measurements of the absolute radar reflectivity. The proposed method used reflectivity differences (in the logarithmic scale); thus, it avoids the calibration problem altogether as well as issues related to wet antennas/radomes. The described retrieval approaches can also be useful for airborne measurements (Walsh et al. 2002) and prospective spaceborne missions such as the Global Precipitation Measurement (GPM), which will have a K_a-band radar aboard the core satellite.

Acknowledgments. This research was supported by the Office of Science (Biological and Environmental Research), U.S. Department of Energy, Grant No. DE-FG02-05ER63954. T. Schneider, M. Shupe, and D. Hazen were members of the NOAA ETL data collection team in the CRYSTAL–FACE field experiment. C. Williams of the NOAA Aeronomy Laboratory provided DSDs collected at the radar site during this experiment. The author thanks Ed Walsh of the NASA Goddard Space Flight Center (the Wallops facility) for fruitful discussions.

REFERENCES

Aydin, K., and S. E. A. Daisley, 2002: Relationships between rainfall rate and 35-GHz attenuation and differential attenuation: Modeling the effects of raindrop size distribution, canting, and oscillation. *IEEE Trans. Geosci. Remote Sens.,* **40,** 2343–2351.

Barber, P., and C. Yeh, 1975: Scattering of electromagnetic waves by arbitrarily shaped dielectric bodies. *Appl. Opt.,* **14,** 2864–2872.

Bohren, C. F., and D. R. Huffman, 1983: *Absorption and Scattering of Light by Small Particles.* John Wiley and Sons, 530 pp.

Brandes, E., G. Zhang, and J. Vivekanandan, 2004: Comparisons of polarimetric radar drop size distribution retrieval algorithms. *J. Atmos. Oceanic Technol.,* **21,** 584–598.

Dong, X., and G. G. Mace, 2003: Profiles of low-level stratus cloud microphysics deduced from ground-based measurements. *J. Atmos. Oceanic Technol.,* **20,** 42–53.

Donovan, D. P., and A. C. A. P. van Lammeren, 2001: Cloud effective particle size and water content profile retrievals using combined lidar and radar observations. Theory and examples. *J. Geophys. Res.,* **106,** 27 425–27 448.

Frisch, A. S., C. W. Fairall, and J. B. Snider, 1995: Measurement of stratus cloud and drizzle parameters in ASTEX with a K_a-band radar and a microwave radiometer. *J. Atmos. Sci.,* **52,** 2788–2799.

Hitschfeld, W., and J. Bordan, 1954: Errors inherent in the radar measurements of rainfall at attenuating wavelengths. *J. Meteor.,* **11,** 58–67.

Iguchi, T., R. Oki, E. A. Smith, and Y. Furuhama, 2002: Global precipitation measurement program and the development of dual-frequency precipitation radar. *J. Commun. Res. Lab.,* **49,** 37–45.

Kropfli, R. A., and Coauthors, 1995: Cloud physics studies with 8 mm wavelength radar. *Atmos. Res.,* **35,** 299–313.

L'Ecuyer, T. S., and G. L. Stephens, 2002: An estimation-based precipitation retrieval algorithm for attenuating radars. *J. Appl. Meteor.,* **41,** 272–285.

Lhermitte, R. M., 1987: A 94 GHz Doppler radar for cloud observations. *J. Atmos. Oceanic Technol.,* **4,** 36–48.

Mace, G. G., T. P. Ackerman, P. Minnis, and D. F. Young, 1998: Cirrus layer microphysical properties derived from surface-based millimeter radar and infrared interferometer data. *J. Geophys. Res.,* **103,** 23 207–23 216.

——, A. J. Heymsfield, and M. R. Poellot, 2002: On retrieving the microphysical properties of cirrus clouds using the moments of the millimeter-wavelength Doppler spectrum. *J. Geophys. Res.,* **107,** 4815, doi:10.1029/2001JD001308.

Matrosov, S. Y., 1999: Retrievals of vertical profiles of ice cloud microphysics from radar and IR measurements using tuned regressions between reflectivity and cloud parameters. *J. Geophys. Res.,* **104,** 16 741–16 753.

——, T. Uttal, J. B. Snider, and R. A. Kropfli, 1992: Estimates of ice cloud parameters from ground-based infrared radiometer and radar measurements. *J. Geophys. Res.,* **97,** 11 567–11 574.

——, A. Korolev, and A. J. Heymsfield, 2002a: Profiling ice mass and characteristic particle size from Doppler radar measurements. *J. Atmos. Oceanic Technol.,* **19,** 1003–1018.

——, K. A. Clark, B. E. Martner, and A. Tokay, 2002b: X-band polarimetric radar measurements of rainfall. *J. Appl. Meteor.,* **41,** 941–952.

——, T. Uttal, and D. A. Hazen, 2004: Evaluation of radar reflectivity-based estimates of water content in stratiform marine clouds. *J. Appl. Meteor.,* **43,** 405–419.

Mead, J. B., A. L. Pazmany, S. M. Sekelsky, and R. E. McIntosh, 1994: Millimeter-wavelength radars for remotely sensing clouds and precipitation. *Proc. IEEE,* **82,** 1891–1906.

Meneghini, R., and T. Kozu, 1990: *Spaceborne Weather Radar.* Artechhouse, 199 pp.

——, K. Nakamura, C. W. Ulbrich, and D. Atlas, 1989: Experimental test of methods for measurements of rainfall rate using an airborne dual-wavelength radar. *J. Atmos. Oceanic Technol.,* **6,** 637–651.

Moran, K. P., B. E. Martner, M. J. Post, R. A. Kropfli, D. C. Welsh, and K. B. Widener, 1998: An unattended cloud-profiling radar for use in climate research. *Bull. Amer. Meteor. Soc.,* **79,** 443–455.

Pasqualucci, F., B. W. Bartram, R. A. Kropfli, and W. R. Moniger, 1983: A millimeter-wavelength dual-polarization Doppler radar for cloud and precipitation studies. *J. Climate Appl. Meteor.,* **22,** 758–765.

Pruppacher, H. R., and R. L. Pitter, 1971: A semi-empirical determination of the shape of cloud and rain drops. *J. Atmos. Sci.,* **28,** 86–94.

Rincon, R. F., R. Lang, R. Meneghini, and S. Bidwell, 2000: Path-average drop size distribution estimation from dual-wavelength measurements of attenuation. *Proc. IGARSS 2000,* Honolulu, HI, IEEE, 184–186.

Smyth, T. J., and A. J. Illingworth, 1997: Estimating rainfall rates at the ground in bright band and non-bright band events. Preprints,

28th Int. Conf. on Radar Meteorology, Austin, TX, Amer. Meteor. Soc., 125–126.

Stephens, G. L., and the CloudSat Science Team, 2002: The CloudSat mission and the A-train. A new dimension of space-based observations of clouds and precipitation. *Bull. Amer. Meteor. Soc.*, **83,** 1771–1790.

Testud, J., E. Le Bouar, E. Obligis, and M. Ali-Mehenni, 2000: The rain profiling algorithm applied to polarimetric weather radar. *J. Atmos. Oceanic Technol.*, **17,** 332–356.

Tokay, A., and D. A. Short, 1996: Evidence from tropical raindrop spectra of the origin of rain from stratiform versus convective clouds. *J. Appl. Meteor.,* **35,** 355–371.

Walsh, E. J., C. W. Wright, D. Vandemark, L. F. Bliven, E. Uhlhorn, P. G. Black, and F. D. Marks Jr., 2002: Rain rate measurement with an airborne scanning radar altimeter. *Proc. IGARSS 2002,* Toronto, ON, Canada, IEEE, 1875–1876.

Wang, Z., and K. Sassen, 2001: Cloud type and microphysical property retrieval using multiple remote sensors. *J. Appl. Meteor.*, **40,** 1665–1682.

White, A. B., J. R. Jordan, B. E. Martner, F. M. Ralph, and B. W. Bartram, 2000: Extending the dynamic range of an S-band radar for cloud and precipitation studies. *J. Atmos. Oceanic Technol.*, **17,** 1226–1234.

Williams, C. R., 2002: Simultaneous ambient air motion and raindrop size distributions retrieved from UHF vertical incident profiler observations. *Radio Sci.*, **37,** 1024, doi:10.1029/2000RS002603.